Possible bipolar effect inducing anomalous transport behavior in the magnetic topological insulator $Mn(Bi_{1-x}Sb_x)_2Te_4$

H. H. Wang,[1] X. G. Luo,[1] M. Z. Shi,[1] K. L. Peng,[1] B. Lei,[1] J. H. Cui,[1] D. H. Ma,[1] W. Z. Zhuo,[1] J. J. Ying,[1] Z. Y. Wang,[1] and X. H. Chen[1,2,3,4,*]

[1]*Key Laboratory of Strongly Coupled Quantum Matter Physics, Chinese Academy of Sciences, Hefei National Laboratory for Physical Sciences at Microscale, Department of Physics, University of Science and Technology of China, Hefei 230026, China*

[2]*Collaborative Innovation Center of Advanced Microstructures, Nanjing University, Nanjing 210093, China*

[3]*CAS Center for Excellence in Superconducting Electronics, Shanghai 200050, China*

[4]*CAS Center for Excellence in Quantum Information and Quantum Physics, Hefei, Anhui 230026, China*

(Received 8 July 2020; revised 25 December 2020; accepted 5 February 2021; published 18 February 2021)

$MnBi_2Te_4$ has attracted tremendous interest as the first discovered intrinsic magnetic topological insulator. Due to its heavily *n*-doped nature, hole doping is required to isolate the effects of the topological states from the bulk, which is necessary for further electronic applications. Here, we systematically measure the resistivity, Seebeck coefficient, and thermal conductivity of $Mn(Bi_{1-x}Sb_x)_2Te_4$ ($0 \leqslant x \leqslant 0.51$) single crystals. We find that the carrier concentrations at room temperature can be continuously tuned from -9.47×10^{19} to 5.21×10^{19} cm^{-3} while varying x from 0 to 0.51. In the crystals with the Fermi level located close to the charge neutral point in the bulk band gap, drastic changes in the resistivity, Seebeck coefficient, and thermal conductivity are observed around a certain temperature T^*. Our results suggest that the bipolar effect possibly plays an important role in determining the transport properties in narrow bulk band topological insulators when the Fermi level is located near the charge neutral point inside the bulk gap.

DOI: 10.1103/PhysRevB.103.085126

I. INTRODUCTION

The interplay of nontrivial band topology and magnetic ordering represents a fertile playground to realize novel physical phenomena, such as the quantum anomalous Hall effect (QAHE), axion insulator states, and magnetic Weyl semimetal states [1–3]. However, the majority of QAHE experiments so far have focused on either magnetic doped topological insulators (TIs) or ferromagnet-TI heterostructures, where the material synthesis and optimization are extremely challenging [4–7]. Therefore, the QAHE was realized only at the very low temperature, making it difficult for practical application. Recently, $MnBi_2Te_4$ has attracted plenty of attention as the first intrinsic antiferromagnetic topological insulator [8,9]. This compound has a layered structure (space group *R*-3*m*) with Te-Bi(Sb)-Te-Mn-Te-Bi(Sb)-Te septuple layers (SLs) stacking along the *c* axis, as shown in Fig. 1(a). $MnBi_2Te_4$ has been theoretically predicted to host a bulk gap of ∼200 meV and Dirac electrons on the surface. Although the Mn atomic layers create A-type antiferromagnetic order in the bulk [10–13], whether a mass gap opens on the surface Dirac spectrum is still under hot debate. On the other hand, the Fermi level of $MnBi_2Te_4$ locates deeply in the bulk conduction band due to its heavily electron-doped nature [9,14], as verified by angle-resolved photoemission spectroscopy (ARPES) measurements [15]. By tuning the chemical potential into the bulk band gap via electric gating, the QAHE and axion insulating state have been realized in 5- and 6-SL samples, respectively [16,17]. Another way to reduce the bulk carriers is to substitute bismuth with antimony. By doping antimony into $MnBi_2Te_4$, the Fermi level can be gradually shifted from the conduction band to the valence band, and the nontrivial band topology remains up to an antimony content of ∼55%, providing a possible path to realize an ideal magnetic topological insulator [18,19].

With continuously doping antimony, many new physical phenomena that differ from $MnBi_2Te_4$ have been predicted and experimentally discovered. A large intrinsic anomalous Hall effect with maximum Hall angle in the ferromagnetic phase driven by external field and a large positive magnetoresistance were observed when the doping level of antimony reached 26%, and an ideal time-reversal symmetry-broken type-II Weyl semimetal was predicted [20]. A ferromagnetic ground state with a Curie temperature of 26 K, in sharp contrast to the antiferromagnetic order in $MnBi_2Te_4$, was found when the doping level of antimony reached 90% [21]. Recently, a strange temperature dependence of resistivity was reported in samples with the Fermi level close to the charge neutral point of the bulk gap (with a Sb doping level about 30%), where a huge resistivity was observed at low temperature, followed by an anomalous drop with rising temperature to ∼130 K [19]. This peculiar behavior in resistivity is not yet fully understood. Considering that such an anomaly has been observed only in the bulk-insulating crystals where the QAHE and axion insulating states might be realized, it is critical to verify the origin of this drastic change in the temperature-dependent resistivity. In this work, we have measured the

*chenxh@ustc.edu.cn

TABLE I. The c-axis lattice parameter c, Néel temperature T_N, room-temperature Hall coefficient R_H, carrier concentration n_H, carrier mobility μ_H, Seebeck coefficient S, thermal conductivity κ, and resistivity ρ at different Sb contents.

Nominal Sb content x	Actual Sb content x	c (Å)	R_H ($cm^3\ C^{-1}$)	n_H ($\times 10^{19}\ cm^{-3}$)	μ_H ($cm^2\ V^{-1}\ s^{-1}$)	$S(T = 300\,K)$ ($\mu V\ K^{-1}$)	$\kappa(T = 300\,K)$ ($W\ K^{-1}\ m^{-1}$)	$\rho(T = 300\,K)$ (mΩ cm)
0	0	40.73	−0.066	−9.47	28.87	−20.2	2.52	2.37
0.1	0.09	40.92	−0.093	−6.74	28.61	−31.1	2.21	3.24
0.2	0.26	40.80	−0.543	−1.15	77.84	−104.8	1.70	6.98
0.2	0.27	40.79	−0.626	−1.00	83.65	35.6	1.95	7.47
0.3	0.35	40.86	0.396	1.58	94.86	68.5	2.21	4.17
0.4	0.41	40.86	0.244	2.56	61.47	97.5	2.24	1.89
0.5	0.51	40.67	0.120	5.21	35.58	81.8	2.44	1.85

resistivity ρ, Seebeck coefficient S, and thermal conductivity κ of single crystals of $Mn(Bi_{1-x}Sb_x)_2Te_4$ ($0 \leqslant x \leqslant 0.51$). Their systematical evolution versus temperature and doping suggests that the bipolar effect could be a possible origin of the anomalous resistivity and Seebeck coefficient in the crystals near the charge neutral point.

II. EXPERIMENT

$Mn(Bi_{1-x}Sb_x)_2Te_4$ ($0 \leqslant x \leqslant 0.51$) single crystals are grown through a self-flux method [18,19]. The high-purity elements manganese, bismuth/antimony, and tellurium are mixed in a ratio of 1:11.7:18.55, where bismuth and antimony are mixed proportionally according to $1-x$:x. The mixed elements are placed in an alumina crucible, and then the alumina crucible is sealed within a quartz ampule. The ampule is slowly heated to 950 °C, kept at this temperature for 1 day, cooled slowly to 595 °C over 2 days, and then held at this temperature for 1 day. Finally, the $Mn(Bi_{1-x}Sb_x)_2Te_4$ single crystals are obtained by centrifugation. Actual chemical compositions are determined by using by an x-ray energy dispersive spectrometer mounted on a field emission scanning electronic microscope (Sirion200). The actual Sb contents of the chosen crystals (with the nominal $x = 0.1$, 0.3, 0.4, and 0.5) for measurements in this work are determined to be 0.09, 0.35, 0.41, and 0.51, respectively. The crystals with the nominal $x = 0.2$ are close to the charge neutral point (as shown in the following text) and are determined to have an actual Sb content of 0.26–0.27, which shows dramatically different transport behavior with only a very slight difference in Sb content. Therefore, two crystals with actual Sb contents of 0.26 and 0.27 are chosen for our investigations. The actual composition will be adopted in the following text.

The single-crystalline x-ray diffraction (XRD) patterns are obtained by using an x-ray diffractometer (SmartLab-9, Rikagu Corp.) with Cu $K\alpha$ radiation. Resistivity and Hall resistivity are measured by using a PPMS-9-Tesla system (Quantum Design). The Seebeck coefficient and thermal conductivity are measured with a home-built setup in a 14T-TeslaTron-PT System (Oxford Instruments) by applying a steady heat current through the crystal [22].

III. RESULTS AND DISCUSSION

Figure 1(b) shows the XRD patterns of $Mn(Bi_{1-x}Sb_x)_2Te_4$ single crystals. The same series of sharp (00l) peaks was found in these patterns, indicating a pure crystalline phase for $Mn(Bi_{1-x}Sb_x)_2Te_4$ with different antimony contents. The lattice parameter c (~40.7–40.9 Å) remains almost unchanged with varying x from 0 to 0.51 (as shown in Table I), consistent with previous reports [18,19].

The Hall resistivity ρ_{xy} for the $Mn(Bi_{1-x}Sb_x)_2Te_4$ crystals with different doping levels at 300 K is shown in Fig. 2(a). A linear magnetic field dependence of ρ_{xy} is observed for all the measured crystals. The Hall coefficient R_H and carrier concentrations n_H at room temperature estimated from $\rho_{xy}(H)$ are displayed in the inset of Fig. 2(a). With increasing Sb content, as shown in the inset in Fig. 2(a), n_H gradually changes from $-9.47 \times 10^{19}\ cm^{-3}$ at $x = 0$ to $5.21 \times 10^{19}\ cm^{-3}$ at $x = 0.51$, with a sign change around $x = 0.3$, indicating that the dominating carriers change from electrons to holes. The extremely low n_H of the crystals with $x = 0.26$ and 0.27 suggests that the Fermi level approaches the charge neutral point of the bulk band gap.

The temperature dependence of the resistivity of these $Mn(Bi_{1-x}Sb_x)_2Te_4$ crystals is shown in Fig. 2(b). Initially, the resistivity of pristine $MnBi_2Te_4$ drops slowly with decreasing temperature, showing a cusplike feature at Néel temperature T_N due to the increase in magnetic scattering caused by spin fluctuations. Below T_N, ρ gradually decreases with decreasing temperature due to the weakening of magnetic scattering after entering the magnetic ordering state. After substituting Bi with Sb, most of the samples show a $\rho(T)$ behavior similar

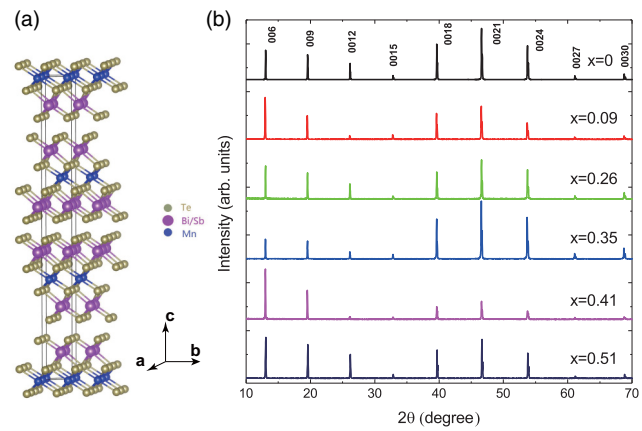

FIG. 1. (a) Crystal structure of the $Mn(Bi_{1-x}Sb_x)_2Te_4$. (b) X-ray diffraction patterns with orientation along the (00l) direction for $Mn(Bi_{1-x}Sb_x)_2Te_4$ crystals.

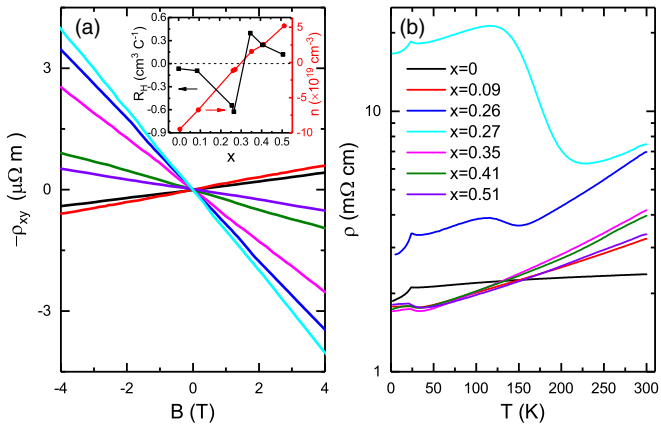

FIG. 2. (a) Magnetic field dependence of the Hall resistivity ρ_{xy} for $Mn(Bi_{1-x}Sb_x)_2Te_4$ crystals measured at 300 K with magnetic fields applied along the c axis. The inset shows the Hall coefficient R_H and carrier concentration n_H of $Mn(Bi_{1-x}Sb_x)_2Te_4$ crystals. (b) Temperature dependence of resistivity ρ for $Mn(Bi_{1-x}Sb_x)_2Te_4$.

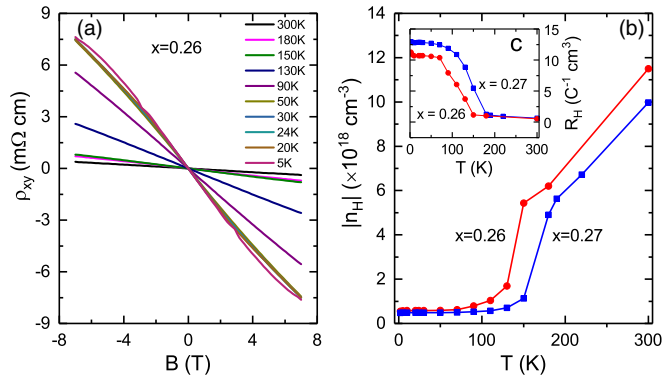

FIG. 3. (a) Hall resistivity taken at various temperatures plotted against magnetic field for $Mn(Bi_{0.74}Sb_{0.26})_2Te_4$ crystals. (b) Temperature dependence of electron-carrier concentration in $Mn(Bi_{0.74}Sb_{0.26})_2Te_4$ and $Mn(Bi_{0.73}Sb_{0.27})_2Te_4$ crystals. (c) Hall coefficient plotted against temperature for $Mn(Bi_{0.74}Sb_{0.26})_2Te_4$ and $Mn(Bi_{0.73}Sb_{0.27})_2Te_4$ crystals.

to that of $MnBi_2Te_4$ except for the crystals with $x = 0.26$ and 0.27. At these two doping levels, the resistivity is much larger at low temperature, which can be attributed to the very low carrier concentrations in these two crystals (consistent with the above indication that the Fermi level of these two crystals is close to the charge neutral point of the bulk band gap, as pointed out above). Above a certain temperature (we denote it as T^*, which is ∼113 K for $x = 0.26$ and ∼117 K for $x = 0.27$), a rapid drop appears in $\rho(T)$. With further increasing temperature, the drop saturates, and essentially, a metallic behavior emerges. Similar resistivity was observed previously in the weak p-doped crystal [19], which has a Sb content of $x = 0.3$, but the origin remains unknown.

Now we focus on the drastic change in the resistivity around 110 K in the crystals with $x = 0.26$ and 0.27. Similar behavior was reported in the sample with $x = 0.30$ (slightly hole doped) and was argued to have a spin-related origin [19]. However, this cannot interpret why such a feature is absent in other crystals with the Fermi level far away from the band gap since there are still an antiferromagnetic transition and spin fluctuations. In order to understand the origin of this peculiar behavior of $\rho(T)$ in those samples, the temperature dependence of the Hall coefficient R_H and Hall carrier density n_H $(=1/eR_H)$ for crystals with $x = 0.26$ and 0.27 is extracted from the Hall resistivity recorded at various temperatures [Fig. 3(a)] and shown in Figs. 3(c) and 3(b). n_H is estimated to be around 0.5×10^{18} cm^{-3} at low temperature, much lower than those in the crystals with $x = 0$–0.09 and 0.35–0.51, indicating that the crystals with $x = 0.26$ and 0.27 have the Fermi level located within the bulk band gap. However, considering the theoretically estimated bulk band gap of ∼80 meV for $x = 0.26$–0.27 [19] and an effective mass of $\sim 0.25 m_e$ [23], the thermally excited carrier density could be about $\sim 10^{16}$ cm^{-3} at 110 K, which is much smaller than the values estimated from Hall data. Therefore, some other origins should be taken into account for these abnormal carrier concentrations. It has been reported that there are two native defects of Mn_{Bi} and Bi_{Te} antisites in pristine $MnBi_2Te_4$ in terms of the topographic images from scanning tunneling microscopy (STM) [10,12,24,25]. These native antisite defects can play an important role in affecting the electronic structure and density of states around the Fermi level [25]. A significant local density of states was observed at ∼100 meV above the bottom of the conduction band in localized triangular regions, resulting from Bi_{Mn} antisites [25]. This suggests that there is a mobility edge in the conduction band and localized states below the mobility edge. As reported, the Fermi level of pristine $MnBi_2Te_4$ is ∼200 meV above the bottom of the conduction band [15], and the Fermi level of $Mn(Bi_{1-x}Sb_x)_2Te_4$ with $x = 0.2$ is located at ∼130 meV [19]. The totally metallic resistivity below 300 K can be observed up to $x = 0.25$ [19]. These facts suggest that the mobility edge is a little higher than 100 meV from the bottom of the conduction band and the localized states induced by the antisite defects lie in the conduction band and are very close to the mobility edge, so that electrons can be easily produced at low temperature by being excited from the localized states to the mobility edge. The existence of a number of electrons on the mobility edge can also interpret the metallic resistivity (positive slope against temperature) in the crystals with $x = 0.26$ and 0.27 at low temperature, even though their Fermi level is within the bulk band gap.

As temperature rises up to T^*, n_H increases rapidly and reaches 5×10^{18} cm^{-3} at 150 K for $x = 0.26$ and at 190 K for $x = 0.27$, followed by a further increase with a much smaller slope. Finally, n_H reaches $\sim 1 \times 10^{19}$ cm^{-3} at room temperature. It suggests that some mechanisms lead to a dramatic enhancement of carrier concentration above T^*, exactly consistent with the rapid drop in $\rho(T)$. Considering that the pronounced change in $n_H(T)$ could lead to a corresponding response in thermoelectric transport, Seebeck coefficients are measured for all the crystals. The temperature dependence of S in temperatures ranging from 10 to 300 K for all the crystals of $Mn(Bi_{1-x}Sb_x)_2Te_4$ is shown in Fig. 4(a). Most of these curves exhibit approximately linear temperature dependence over the whole temperature range except for the crystals with $x = 0.26$ and 0.27. S of the crystals with $x = 0.26$ and 0.27

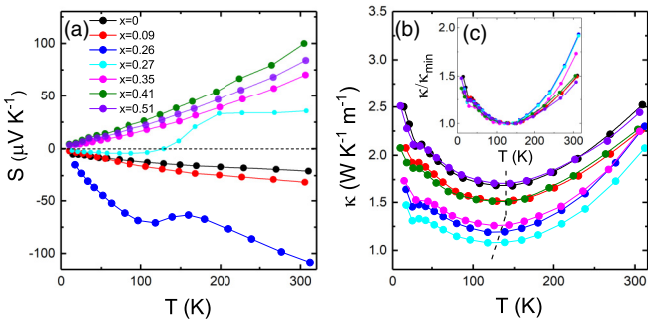

FIG. 4. Temperature dependence of (a) the Seebeck coefficient, (b) thermal conductivity κ, and (c) $\kappa/\kappa_{\min}$ shown in the temperature range from 10 to 310 K for $Mn(Bi_{1-x}Sb_x)_2Te_4$ crystals. The dotted lines sketch out the evolution of the corresponding temperature of the minimum in $\kappa(T)$ with varying Sb content.

shows increasing negative values at low temperature with increasing temperature and begins to decrease in absolute value as temperature rises up to T^*. This is consistent with a rapid drop in $\rho(T)$ and enhancement in $n_H(T)$. For the crystal with $x = 0.27$, S even changes sign from negative to positive as temperature rises across 131 K. At room temperature, as shown in Fig. 4(a), S has a value of $-20.2\,\mu$V K^{-1} for $x = 0$. As the Sb content increases, S has a negative maximum of $-104.8\,\mu$V K^{-1} at $x = 0.26$, changes from negative to positive for $x = 0.27$, and reaches a positive maximum of $97.5\,\mu$V K^{-1} for $x = 0.41$. The evolution of sign and absolute values in S is also consistent with the Hall coefficient. The absolute values of S reach the maxima as the Fermi level locates close ($x = 0.26$) but not too close (like $x = 0.27$) to the charge neutral point of the bulk band gap.

We also find anomalous behavior at almost the same temperature in the temperature dependence of thermal conductivity. In Fig. 4(b), κ of all the $Mn(Bi_{1-x}Sb_x)_2Te_4$ crystals is plotted against temperature below 310 K. κ shows weak temperature dependence in the whole temperature range and exhibits a shallow dip around T_N. This kind of diplike feature near the magnetic transition temperature was also observed in $La_{0.8}Ca_{0.2}MnO_3$ and CoF_2 due to the scattering of the phonons by critical spin fluctuations [26,27]. Spin fluctuations impede the heat flow of phonons and fail to hinder the heat flow of the carrier, resulting in the reduction of lattice thermal conductivity [26,27]. Surprisingly, κ gradually increases above a certain temperature (~115–120 K, close to T^*) for all the crystals with increasing temperature, which cannot be explained by either the general lattice thermal conductivity (in the high-temperature range above the Debye temperature (110 K for $MnBi_2Te_4$ [28]), the lattice thermal conductivity κ_L is mainly dominated by the umklapp process and obeys $\kappa_L \propto 1/T$ behavior) or electronic thermal conductivity (which can be estimated from the Wiedemann-Franz law $\kappa_e/\sigma = LT$, with L being the Lorenz number and $\sigma = 1/\rho$ being the electrical conductivity). In order to more clearly see the systematic change of the temperature dependence of the thermal conductivity for various x, $\kappa/\kappa_{\min}$ is plotted against temperature for all the crystals, as shown in Fig. 4(c). As can be seen, $\kappa/\kappa_{\min}$ for crystals with $x = 0$, 0.09, 0.41, and 0.51 have almost the same temperature dependence, while for the crystals with $x = 0.26$, 0.27, and 0.35, there is a relatively enhanced part at elevated temperature. In $MnBi_2Te_4$, a large number of native Mn_{Bi} and Bi_{Te} antisite defects have been found by STM and x-ray diffraction [10,12,24,25], which can result in glasslike enhanced thermal conductivity at elevated temperature (for the crystals with $x = 0$, 0.09, 0.41, and 0.51) [10,29–31]. For the additional increased part in the thermal conductivity at elevated temperatures for the crystals with $x = 0.26$, 0.27, and 0.35, the bipolar effect can be taken into account as a possible interpretation [32,33]. The bipolar effect usually becomes important at high temperature in narrow-band-gap semiconductors or zero-band-gap semiconductors (semimetals) [33,34]. The pairs of thermally excited electrons and holes will diffuse from the hotter region to the colder region if a temperature difference is established, with additional heat conduction through the movements of carriers and the energy release on the colder side due to annihilation of electron and hole pairs [33,34]. The bipolar effect has been used to interpret the increasing thermal conductivity at elevated temperature in narrow-band semiconductors (e.g., $BiTe_2Se$ with a bulk band gap ~300 meV [35]) and semimetals (e.g., the Dirac semimetal Cd_3As_2 [22]). In a semiconductor with a relatively small bulk band gap (~80 meV for $x = 0.26$–0.27), the bipolar effect can be naturally taken into account for interpreting the increasing thermal conductivity at elevated temperature, as observed here. The increasing thermal conductivity can be more pronounced when the Fermi level approaches the charge neutral point of the bulk gap, where $\sigma_p \approx \sigma_n$ is achieved. As shown in Fig. 4(b), the onset temperature of the bipolar effect (as indicated by the dotted lines) becomes lower, and the enhancement of the thermal conductivity (the ratio of κ at 300 K to the minimum) gets larger when the system shifts to the charge neutral point.

Taking the bipolar effect into account, we now discuss the anomalous behaviors of $\rho(T)$ and $S(T)$ in crystals with $x = 0.26$ and 0.27. In narrow-band semiconductors, pairs of holes and electrons can be excited at elevated temperature due to the bipolar effect, which will add an extra contribution to the total electrical conductivity and therefore give rise to a drastic drop in $\rho(T)$. As one can see in Fig. 2(b), the drop in $\rho(T)$ is quickly reduced as Fermi level shifts a little farther away from the charge neutral point (just as x changes from 0.27 to 0.26). Therefore, although there is an enhancement of thermal conductivity at elevated temperature for the crystal with $x = 0.35$ due to the bipolar effect, no effect can be observed in $\rho(T)$ because the Fermi surface of this specimen has just moved out of the bulk band gap.

In the presence of the bipolar effect, there are two types of carriers above T^*, and the intrinsically excited holes and electrons will contribute to the total S together with the extrinsically doped carriers. As a result, the total S can be expressed as $S_{tot} = \frac{S_e\sigma_e + S_p\sigma_p}{\sigma_e + \sigma_p}$ [34] (the subscript e refers to the electron carriers, including the intrinsically excited and extrinsically doped ones in the crystals with $x = 0.26$ and 0.27 here, and the subscript p represents the intrinsically excited holes). In the crystals with $x = 0.26$ and 0.27, since the crystals locate on the electron-doped side, the reduction in $|S|$ at $x = 0.26$ and the sign change in S with $x = 0.27$ at elevated temperature can be ascribed to the contribution from the larger

thermopower contribution from the intrinsically excited holes compared to that from the intrinsically excited electrons.

As can be noted, the obvious changes in $\rho(T)$ and $S(T)$ can be observed only in the crystals with the Fermi level located close to the charge neutral point of the bulk band gap, in which the concentrations of the excited holes and electrons can be comparable to or even larger than the carrier concentration from doping. As suggested by the evolution of $n_H(T)$ shown in Fig. 3(b), the number of intrinsically excited holes and electrons seems to be much larger than that of the external doped electrons for the crystals with $x = 0.26$ and 0.27. In this case, it is reasonable that the bipolar effect can lead to the remarkable changes in $\rho(T)$ and $S(T)$ for the crystals with $x = 0.26$ and 0.27. Similar anomalous behaviors of transport properties were observed in the $ZrTe_5$ crystal grown by the chemical vapor transport method [36], where a drop in resistivity and sign change in the Seebeck coefficient take place at about 130 K. Recently, such phenomena were interpreted by considering the bipolar effects [36–39]. Next, we discuss why one cannot find any similar anomaly in $\rho(T)$ and $S(T)$ in other crystals since the change in n_H due to the bipolar effect is quite large and reaches $\sim 1 \times 10^{18}$ cm^{-3}, calculated by the thermal activation formula with $\sim 0.25 m_e$ effective mass and ~80 meV bulk band gap [19,23]. As intrinsically excited electrons and holes emerge due to the bipolar effect, the Hall coefficient should be written as $R_H = \frac{R_e\sigma_e^2 + R_p\sigma_p^2}{(\sigma_e+\sigma_p)^2}$ (the subscripts e and p refer to the same carriers as described above). Because the sign of R_p is opposite that of R_e, the obtained R_H is smaller than that expected by considering purely electron carriers. Consequently, the estimated n_H at high temperature (above T^*) in Fig. 3(b) is larger than the actual number of the carriers (the sum of hole and electron carriers). Therefore, the concentrations of the intrinsically excited holes and electrons could be much smaller than $\sim 1 \times 10^{19}$ cm^{-3} at room temperature (but comparable to or larger than the external doped carrier concentration in the crystals with $x = 0.26$ and 0.27) and certainly much smaller than the external doped electrons or holes in the crystals with $x = 0$, 0.09, and 0.35–0.51. As a consequence, the contribution from the intrinsically excited carriers has a negligible effect on the electrical conductivity and Seebeck coefficient in the crystals with $x = 0$, 0.09, and 0.35–0.51. Our work suggests that the combination of the Seebeck coefficient and thermal conductivity is helpful for understanding the peculiar behavior in electrical transport. Finally, we also want to mention that the composition inhomogeneity might possibly induce the anomalous behavior observed in $\rho(T)$ and Hall coefficient since it is actually inevitable for alloys like $Mn(Bi,Sb)_2Te_4$. But it also should be noted that the dramatic change in thermopower in the crystals with $x = 0.26$ and 0.27 is difficult to understand in terms of only the composition inhomogeneity.

In addition, the Lifshitz transition might also be considered as one possibility for interpreting such peculiar behavior in resistivity and thermopower. It has been reported that as the temperature changes from low temperature to high temperature in the $ZrTe_5$ crystal, a Lifshitz transition takes place, and its Fermi level moves from the conduction band to the valence band, which results in an anomalous resistivity peak and change in the sign of the thermopower [40,41]. The dramatic reduction in resistivity and thermopower in $Mn(Bi_{1-x}Sb_x)_2Te_4$ crystals with $x = 0.26$ and 0.27 here might also be similarly attributed to a Lifshitz transition associated with the temperature-dependent chemical potential. However, there has been no report of a Lifshitz transition in the $Mn(Bi_{1-x}Sb_x)_2Te_4$ system yet, and further experiments (such as temperature-dependent ARPES measurements) are required to clarify whether a Lifshitz transition exists in this material system. Furthermore, in the picture of a Lifshitz transition, it is hard to understand the additional enhancement in the thermal conductivity for the crystals with $x = 0.26$ and 0.27 relative to those for the other compositions of crystals at elevated temperature [as shown in Fig. 4(c)] since the electronic thermal conductivity arising from conduction carriers can be estimated by the Wiedemann-Franz law to be only ~ 0.1 W K^{-1} m^{-1} at 300 K for the crystals with $x = 0.26$ and 0.27, which is far less than the relatively enhanced part of 0.5 W K^{-1} m^{-1}. More experimental and theoretical works are needed to achieve comprehensive understanding of the anomalous transport behaviors in $Mn(Bi_{1-x}Sb_x)_2Te_4$ crystals.

IV. CONCLUSION

We have systematically measured the electrical resistivity, Seebeck coefficient, and thermal conductivity of $Mn(Bi_{1-x}Sb_x)_2Te_4$ single crystals in a large doping range. Anomalous changes can be observed in the resistivity and Seebeck coefficient for the crystals with the Fermi level lying close to the charge neutral point in the bulk band gap. Combined with the abnormal behavior in thermal conductivity, such peculiar behavior in the resistivity and Seebeck coefficient can be well understood by taking into account the bipolar effect. Our work suggests that the bipolar effect could be considered for a full understanding of the electrical, thermoelectric, and thermal transport properties in topological materials with the Fermi level approaching the charge neutral point in the bulk band gap.

ACKNOWLEDGMENTS

This work was supported by the Anhui Initiative in Quantum Information Technologies (Grant No. AHY160000), the National Key Research and Development Program of the Ministry of Science and Technology of China (Grants No. 2019YFA0704901, No. 2016YFA0300201, and No. 2017YFA0303001), the Science Challenge Project of China (Grant No. TZ2016004), the Key Research Program of Frontier Sciences, CAS, China (Grant No. QYZDYSSW-SLH021), the Strategic Priority Research Program of the Chinese Academy of Sciences (Grant No. XDB25000000), and the National Natural Science Foundation of China (Grants No. 11888101 and No. 11534010).

[1] R. Yu, W. Zhang, H. J. Zhang, S. C. Zhang, X. Dai, and Z. Fang, Science **329**, 61 (2010).

[2] R. D. Li, J. Wang, X. L. Qi, and S. C. Zhang, Nat. Phys. **6**, 284 (2010).

[3] X. G. Wan, A. M. Turner, A. Vishwanath, and S. Y. Savrasov, Phys. Rev. B **83**, 205101 (2011).

[4] C. Z. Chang *et al.*, Science **340**, 167 (2013).

[5] C. Z. Chang, W. W. Zhao, Duk Y. Kim, H. J. Zhang, A. Assaf, D. Heiman, S. C. Zhang, C. X. Liu, H. W. Chan, and S. Moodera, Nat. Mater. **14**, 473 (2015).

[6] Y. L. Chen, J. H. Chu, J. G. Analytis, Z. K. Liu, K. Igarashi, H. H. Kuo, X. L. Qi, S. K. Mo, R. G. Moore, D. H. Lu, M. Hashimoto, T. Sasagawa, S. C. Zhang, I. R. Fisher, Z. Hussain, and Z. X. Shen, Science **329**, 659 (2010).

[7] D. Xiao, J. Jiang, J. H. Shin, W. Wang, F. Wang, Y. F. Zhao, C. Liu, W. Wu, M. H. W. Chan, N. Samarth, and C. Z. Chang, Phys. Rev. Lett. **120**, 056801 (2018).

[8] J. H. Li, Y. Li, S. Q. Du, Z. Wang, B. L. Gu, S. C. Zhang, K. He, W. H. Duan, and Y. Xu, Sci. Adv. **5**, 5685 (2019).

[9] M. M. Otrokov *et al.*, Nature (London) **576**, 416 (2019).

[10] J. Q. Yan, Q. Zhang, T. Heitmann, Z. Huang, K. Y. Chen, J. G. Cheng, W. D. Wu, D. Vaknin, B. C. Sales, and R. J. McQueeney, Phys. Rev. Materials **3**, 064202 (2019).

[11] P. Swatek, Y. Wu, L. L. Wang, K. Lee, B. Schrunk, J. Q. Yan, and A. Kaminski, Phys. Rev. B **101**, 161109(R) (2020).

[12] A. Zeugner *et al.*, Chem. Mater. **31**, 2795 (2019).

[13] D. A. Estyunin, I. I. Klimovskikh, A. M. Shikin, E. F. Schwier, M. M. Otrokov, A. Kimura, S. Kumar, S. O. Filnov, Z. S. Aliev, M. B. Babanly, and E. V. Chulkov, APL Mater. **8**, 021105 (2020).

[14] S. H. Lee, Y. Zhu, Y. Wang, L. Miao, T. Pillsbury, H. Yi, S. Kempinger, J. Hu, C. A. Heikes, P. Quarterman, W. Ratcliff, J. A. Borchers, H. Zhang, X. Ke, D. Graf, N. Alem, C. Z. Chang, N. Samarth, and Z. Mao, Phys. Rev. Research **1**, 012011(R) (2019).

[15] Y. J. Chen, L. X. Xu, J. H. Li, Y. W. Li, H. Y. Wang, C. F. Zhang, H. Li, Y. Wu, A. J. Liang, C. Chen, S. W. Jung, C. Cacho, Y. H. Mao, S. Liu, M. X. Wang, Y. F. Guo, Y. Xu, Z. K. Liu, L. X. Yang, and Y. L. Chen, Phys. Rev. X **9**, 041040 (2019).

[16] Y. J. Deng, Y. J. Yu, M. Z. Shi, Z. X. Guo, Z. H. Xu, J. Wang, X. H. Chen, and Y. B. Zhang, Science **367**, 895 (2020).

[17] C. Liu, Y. C. Wang, H. Li, Y. Wu, Y. X. Li, J. H. Li, K. He, Y. Xu, J. S. Zhang, and Y. Y. Wang, Nat. Mater. **19**, 522 (2020).

[18] J. Q. Yan, S. Okamoto, M. A. McGuire, A. F. May, R. J. McQueeney, and B. C. Sales, Phys. Rev. B **100**, 104409 (2019).

[19] B. Chen *et al.*, Nat. Commun. **10**, 4469 (2019).

[20] S. H. Lee, Y. L. Zhu, H. Yi, D. Graf, R. Basnet, A. Fereidouni, A. Wegner, Y. F. Zhao, L. J. Min, K. Verlinde, J. Y. He, R. Redwing, H. H. Churchill, N. Samarth, C. Z. Chang, J. Hu, and Z. Q. Mao, arXiv:2002.10683.

[21] Y. Y. Chen, Y.-W. Chuang, S. H. Lee, Y. Zhu, K. Honz, Y. Guan, Y. Wang, K. Wang, Z. Mao, J. Zhu, C. Heikes, P. Quarterman, P. Zajdel, J. A. Borchers, and W. Ratcliff II, Phys. Rev. Mater. **4**, 064411 (2020).

[22] H. H. Wang, X. G. Luo, K. L. Peng, Z. L. Sun, M. Z. Shi, D. H. Ma, N. Z. Wang, T. Wu, J. J. Ying, Z. F. Wang, and X. H. Chen, Adv. Funct. Mater. **29**, 1902437 (2019).

[23] Ch. X. Trang, Q. Li, Y. Yin, J. Hwang, G. Akhgar, I. D. Bernardo, A. Grubišić-Čabo, A. Tadich, M. S. Fuhrer, S. Mo, N. Medhekar, and M. T. Edmonds, arXiv:2009.06175.

[24] Y. Yuan, X. Wang, H. Li, J. Li, Y. Ji, Z. Hao, Y. Wu, K. He, Y. Wang, Y. Xu, W. Duan, W. Li, and Q. K. Xue, Nano Lett. **20**, 3271 (2020).

[25] Z. Huang, M.-H. Du, J. Yan, and W. Wu, Phys. Rev. Mater. **4**, 121202(R) (2020).

[26] H. Stern, J. Phys. Chem. Solids **26**, 153 (1965).

[27] B. X. Chen, A. G. Rojo, C. Uher, H. L. Ju, and R. L. Greene, Phys. Rev. B **55**, 15471 (1997).

[28] J.-Q. Yan, Y. H. Liu, D. S. Parker, Y. Wu, A. A. Aczel, M. Matsuda, M. A. McGuire, and B. C. Sales, Phys. Rev. Mater. **4**, 054202 (2020).

[29] Y. Suemune and H. Ikawa, J. Phys. Soc. Jpn. **19**, 1686 (1964).

[30] J. L. Cohn, G. S. Nolas, V. Fessatidis, T. H. Metcalf, and G. A. Slack, Phys. Rev. Lett. **82**, 779 (1999).

[31] B. C. Sales, B. C. Chakoumakos, R. Jin, J. R. Thompson, and D. Mandrus, Phys. Rev. B **63**, 245113 (2001).

[32] J. A. Krumhiansl, J. Phys. Chem. Solids. **8**, 343 (1959).

[33] H. J. Goldsmid, Proc. Phys. Soc., London, Sect. B **69**, 203 (1956); *Introduction to Thermoelectricity* (Springer, Berlin, 2010).

[34] H. Yoshino and K. Murata, J. Phys. Soc. Jpn. **84**, 024601 (2015).

[35] Z. Luo, J. F. Tian, S. Y. Huang, M. Srinivasan, J. Maassen, Y. P. Chen, and X. F. Xu, ACS Nano **12**, 1120 (2018).

[36] P. Shahi, D. J. Singh, J. P. Sun, L. X. Zhao, G. F. Chen, Y. Y. Lv, J. Li, J. Q. Yan, D. G. Mandrus, and J. G. Cheng, Phys. Rev. X **8**, 021055 (2018)

[37] Q. Li, D. Kharzeev, C. Zhang, Y. Huang, I. Pletikosi, A. V. Fedorov, R. D. Zhong, J. A. Schneeloch, G. D. Gu, and T. Valla, Nat. Phys. **12**, 550 (2016).

[38] T. Liang, J. J. Lin, Q. Gibson, S. Kushwaha, M. Liu, W. Wang, H. Xiong, J. Sobota, M. Hashimoto, P. Kirchmann, Z. X. Shen, R. J. Cava, and N. P. Ong, Nat. Phys. **14**, 451 (2018).

[39] R. Y. Chen, S. J. Zhang, J. A. Schneeloch, C. Zhang, Q. Li, G. D. Gu, and N. L. Wang, Phys. Rev. B **92**, 075107 (2015).

[40] Y. Zhang *et al.*, Nat. Commun. **8**, 15512 (2017).

[41] H. Chi, C. Zhang, G. Gu, D. E. Kharzeev, X. Dai, and Q. Li, New J. Phys. **19**, 015005 (2017).